TOPICAL REVIEW — 2D materials: physics and device applications

Graphene integrated photodetectors and opto-electronic devices — a review*

Xiaomu Wang(王肖沐)[1,†] and Xuetao Gan(甘雪涛)[2,‡]

[1] School of Electronic Science and Engineering, Nanjing University, Nanjing 210023, China
[2] School of Science, Northwestern Polytechnical University, Xi'an 710072, China

(Received 20 September 2016; revised manuscript received 23 November 2016; published online 18 January 2017)

Graphene and other two-dimensional materials have recently emerged as promising candidates for next-generation, high-performance photonics. In this paper, the progress of research into photodetectors and other electro-optical devices based on graphene integrated silicon photonics is briefly reviewed. We discuss the performance metrics, photo-response mechanisms, and experimental results of the latest graphene photodetectors integrated with silicon photonics. We also lay out the unavoidable performance trade-offs in meeting the requirements of various applications. In addition, we describe other opto-electronic devices based on this idea. Integrating two-dimensional materials with a silicon platform provides new opportunities in advanced integrated photonics.

Keywords: two-dimensional materials, photodetector, integrated photonics

PACS: 42.82.–m, 78.67.Wj, 85.60.–q **DOI:** 10.1088/1674-1056/26/3/034203

1. Introduction

Photonic technologies have now replaced electronics in long-distance extra-large-scale data links. With engineers inspired by this success, their designs for next-generation network interconnects, in forms of both intra- and on-chip data links, require optical connections of growing complexity and scaled-down costs.[1,2] Over the past decade, silicon photonics, mainly based on the silicon-on-insulator (SOI), has rapidly blossomed because of attractive performance and compact footprints.[3,4] The rationale of applying integrated silicon photonics as network interconnects is many-faceted. The miniature footprint facilitates photons by reduced size and power consumption. In addition, a state-of-the-art SOI platform offers a full set of photonic components – modulators, photo-detectors, filters, multiplexers, splitters, etc. The SOI fabrication process is CMOS technology compatible, permitting high chip yield and reliability, and low manufacturing cost. Furthermore, optical and electrical interfaces are easily combined by means of integrated photonics. This phenomenon effectively reduces packaging costs at the system level. Finally, while telecommunication and interconnects are major drivers in the development of integrated photonics, photonic integration is also recognized as important for potential solutions in other fields, such as distributed sensor networks, disposable medical diagnostic chips, and bio-imaging systems.[5,6]

Hybrid silicon platforms that heterogeneously integrate an SOI platform with other functional materials (such as germanium and III/V semiconductors) provide new opportunities for applying integrated photonics. For instance, heterogeneous integration of narrow bandgap indium-phosphide can make an SOI platform outperform traditional silicon devices – enabling more efficient modulators, faster photo-detectors, on-chip laser diodes, and semiconductor-based optical amplifiers.[7–9] These improvements enhance the functionality of integrated photonic systems and give designers flexibility in choosing between available components. However, several technological limitations of hybrid silicon platforms continue to hamper their application. Growing these high-quality, bulk semiconductors is today an expensive and complex epitaxial process, which contributes heavily to the overall fabrication cost. In addition, these materials are generally hard to integrate with silicon. Extra bonding processes further hinder their usage. Finally, so far, only a finite set of materials have been successfully used in the hybrid systems. The narrow selection range of materials restricts practical applications.

Graphene and other 2D materials have several major advantages over the traditional bulk semiconductors.[10] Here, 2D means layered materials only a few atoms thick. First, the surface of graphene is chemically passivated, supporting free integration with an arbitrary substrate. This inherent integratability easily permits integrated photonic device performance to benefit from intriguing properties and functionalities of 2D materials and their van der Waals heterojunctions. Second, the ultra thin geometry in the out-of-plane direction results in strong quantum confinement, giving rise to numerous never-

*Project supported by the National Natural Science Foundation of China (Grant Nos. 61522507 and 11404264).
†Corresponding author. E-mail: xiaomu.wang@nju.edu.cn
‡Corresponding author. E-mail: xuetaogan@nwpu.edu.cn
© 2017 Chinese Physical Society and IOP Publishing Ltd

before-seen physical properties that do not exist in the bulk forms.[11,12] Third, together, graphene and other 2D materials offer a wide range of bandgaps. This large energy coverage corresponds to a broad electromagnetic spectral range (from far infrared to ultra-violet), which is highly desirable and beyond the spectral coverage of all other semiconductors to date.

Graphene, the first 2D semiconductor to be realized, is a gapless semimetal.[13,14] Hence, it interacts with long-wavelength light (even microwave), and therefore is a highly desirable update to silicon that provides much of the spectral range of SOI platforms. In this review, we discuss recent progress of research into photodetectors and other electro-optical devices based on graphene integrated silicon photonics. First, we focus on the status of integrated graphene photodetectors. In Section 2, we briefly discuss the metrics used to evaluate the performance of photodetectors. We stress the importance of trade-offs between various metrics as well as the necessity of adjusting the metrics' relative priorities according to specific applications. In Section 3, we discuss the physical mechanism of photo-detection in graphene. In Section 4, we present the latest experimental implementation (mainly performance boosters and their design principles) of graphene integrated photodetectors. We then go into the details of other graphene integrated photonic devices such as modulators and light sources in Section 5. Finally, we conclude our paper with current challenges and future opportunities in Section 6.

2. Performance metrics of photodetectors

Several figures of merit (FOMs) are used to evaluate the performance of a photodetector, including responsivity, quantum efficiency, detectivity, and operating speed. In addition to these standard characteristics, several metrics involving fabrication and operation such as cost and power consumption are also important.

Responsivity is one of the most important characteristics for a photodetector. It is defined as the photocurrent $I_{\rm ph}$ divided by the incident light power $P_{\rm in}$, $R = I_{\rm ph}/P_{\rm in}$; or equally defined as photovoltage $V_{\rm pc}$ divided by $P_{\rm in}$, $R = V_{\rm pc}/P_{\rm in}$, if the voltage is measured. Responsivity commonly features the sensitivity of converting optical input to electrical output. For a typical monolayer graphene detector, responsivity is limited to a few mA/W. As shown below, integrating graphene with silicon photonics could significantly enhance the responsivity to around 1 A/W. It is worth mentioning that the definition can be easily expanded to include wavelength dependence. Broadband photo-detection requires flat responsivity across a large spectral range, while single-color detectors call for a sharp peak in a narrow range. In a system that responds linearly to optical input, responsivity is power-independent, which is also practically desirable. Responsivity can equivalently be described by quantum efficiency. The external quantum efficiency (EQE) is equal to the number of electron–hole pairs collected to generate photocurrent in unit time divided by the number of incident photons in the same time: $\mathrm{EQE} = (I_{\rm ph}/q)/(P_{\rm in}/E_{\rm ph})$, where q is the electron charge and $E_{\rm ph}$ is the incident photon energy. Internal quantum efficiency (IQE) is defined in a similar way, except that the absorbed photon number is considered instead of the incident photon number as in EQE. That is, $\mathrm{IQE} = (I_{\rm ph}/q)/(A_{\rm abs}P_{\rm in}/E_{\rm ph})$, where $A_{\rm abs}$ is the absorption coefficient in a given wavelength. Photodetectors are often benchmarked by their optical gain, which is defined as the number of carriers detected for each single incident photon. In photogating contexts, optical gain can alternatively be quantitatively expressed by the ratio of the lifetime of the trapped carriers to the drift transport time, $G_{\rm opt} = \tau_{\rm tr}/\tau_{\rm transit}$. $\tau_{\rm tr}$ is an intrinsic feature of trap states, $\tau_{\rm transit}$ is determined by carrier mobility μ and accelerated electric field (or equivalently, bias voltage V): $\tau_{\rm transit} = L^2/\mu V$, where L is the channel length.

Specific detectivity and noise equivalent power (NEP) are always used to characterize the minimum detectable signal of a photodetector. NEP is the signal power in which the signal-to-noise is unity. NEP generally depends on the noise power density Sn and responsivity of a photodetector, $\mathrm{NEP} = Sn/R$. Specific detectivity is defined as $D = (Af_{\rm BW})^{0.5}/\mathrm{NEP}$, where A is the detector area and $f_{\rm BW}$ is the frequency bandwidth. The unit is Jones, or cm·Hz$^{0.5}$/W. Specific detectivity describes the minimum detectable signal of a photodetector. A large specific detectivity is useful for detecting weak signals. High responsivity (10^{11}–10^{13} Jones) is required for applications such as sensing and telecommunications in which the light signal may be weak. In particular, for certain applications such as IR detection, the predominant noise sources are very temperature-dependent. Thus, operating a photo-detector in low temperatures significantly promotes detectivity. These detectors generally require cryocooling.

Operating speed commonly characterizes photodetectors' ability to detect a signal at certain rate. In frequency domain, the speed features (3 dB) bandwidth of a photodetector, which is always defined by the frequency at which responsivity is reduced to 50% of its maximum value. In the time domain, response time is used. It is defined as the time required for a transient output signal to reach 0.707 of its steady-state change, when the input light changes abruptly. For some systems, the response time may be asymmetric between light switch ON and OFF. In this scenario, response speeds are separately specified by rise- and fall-time. Fast operation (up to tens of GHz) is extremely important for telecommunication and interconnection, but for other applications such as sensing and imaging, only moderate speed (a few kHz) is required.

Power consumption is also particularly important for certain applications, such as in interconnects and remote sensing.

These applications generally require photo-detectors that consume power on the order of pW/bit. For photoconductive detectors, static power consumption resulting from dark current is the major power consumption source. In particular, for a graphene channel, the vanishing bandgap leads to high conductivity and large dark current. Suppressing dark current is one of the key tasks in graphene-based photo-detection.

In addition to the "intrinsic" metrics of photodetectors, fabrication cost has become particularly important. Fabrication of photodetectors involves several processes. The first step is preparing materials. Low cost, environmental safety, and ability to integrate with other semiconductors are highly desired for photodetectors. We will discuss related issues specific to different devices in the following sections. The fabrication process limits the total cost as well as the application of photodetectors. In addition to the standard etching patterning and thin film growth processes, photodetectors based on non-integrable materials call for extra, expensive post-processes such as bonding, especially for focus plane arrays. Two-dimensional materials thus have a significant advantage for this kind of application. Another important feature is the device footprint. Miniaturized device size is generally required for on-chip interconnections and telecommunications.

In most cases, the FOMs discussed above have trade-offs. For instance, although reducing the footprint of a photodetector may increase its operating speed, while reducing its power consumption and total noise floor, the reduction of total incident light flux could also reduce responsivity. Similarly, overall responsivity can be significantly boosted by embedding detectors into photonic structures as will be discussed later, but at the cost of increased complexity and fabrication cost. Although this review mainly discusses the impact and performance of integrated graphene photodetectors, the performance metrics discussed in this section can be generally expanded to evaluate intrinsic performance of photodetectors based on other 2D and bulk materials.

3. Photodetection in graphene

A photodetector is a device that converts absorbed photons into an electrical output signal. A typical graphene photodetector is depicted in Fig. 1(a). Photodetection in graphene can be categorized into five main classes: photovoltaic effect, photo-thermoelectric effect, bolometric effect, plasma-wave-assisted mechanism, and photogating effect.[15–17]

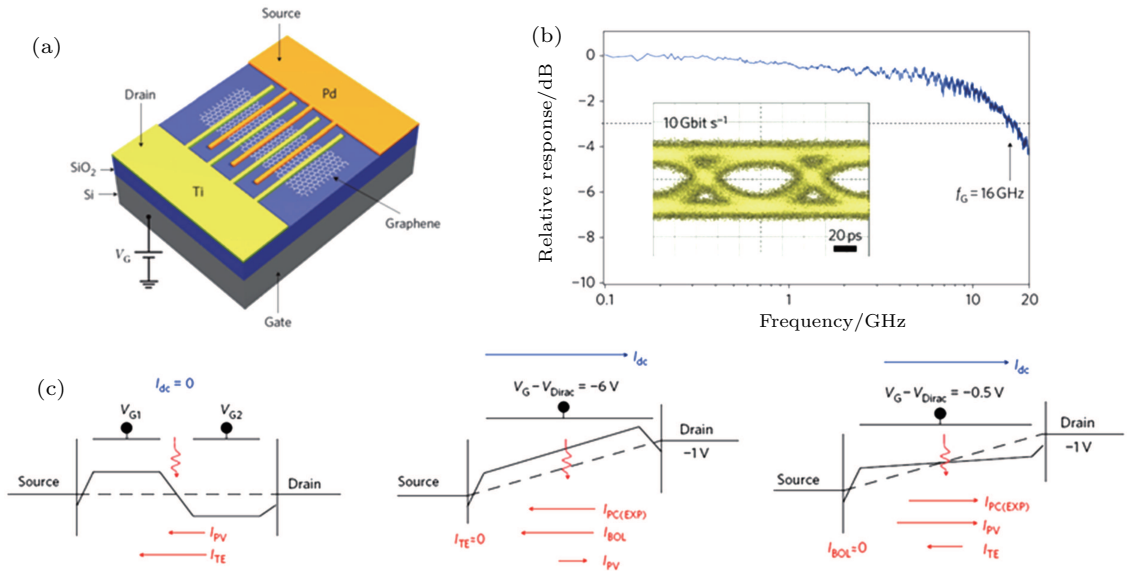


Fig. 1. (color online) Graphene MSM photodetector. (a) Three-dimensional schematic of a graphene MSM photodetector. (b) Relative photoresponse versus light intensity modulation frequency. The 3-dB bandwidth of this photodetector is above 15 GHz. Inset: receiver eye-diagram obtained using this photodetector, showing a clear open eye (from Ref. [29]). (c) (Left) Energy band diagram of a graphene p–n junction used in typical photocurrent measurements. With zero bias, dc current and the bolometric current are zero. Thermoelectric and photovoltaic currents point in the same direction. (Middle) and (Right) Energy band diagrams for graphene MSM photodetector. A uniform graphene channel is subjected to a finite source–drain bias, under small and high doping levels, respectively. Thermoelectric (TE) and photovoltaic (PV) currents are opposite. At low electrostatic doping, the photovoltaic effect dominates, while at high doping levels, the bolometric effects are pronounced (from Ref. [28]).

3.1. Photovoltaic effect

Photocurrent is generated by separating photon-induced electron–hole pairs. The separation can be driven either by the built-in electric field (within a p–n junction or a metal–semiconductor Schottky junction) or an externally applied bias field, as demonstrated in Fig. 1(c).[18,19] In graphene detectors, external bias voltage is not desired because it results in very high dark current and higher power consumption. Graphene p–n junctions can be created by multiple methods, such as local chemical doping,[20] splitting gate structures,[21] or inherent work function differences between graphene with different layers.[22] Photovoltaic photocurrent is controlled by

the junction. Its direction depends only on the direction of the electric field. It is also worth mentioning that, owing to the zero bandgap, strong carrier–carrier scattering results in Auger-type impact ionization or carrier multiplication, i.e., multiple electron–hole pairs are generated by a single photon when the photo-excited electrons and holes quickly thermalize in the conduction and valence bands.[23–25] Carrier multiplication can occur in zero bias. It can potentially boost photodetection efficiency.[26,27] On the other hand, this process is fundamentally different from the impact ionization in traditional semiconductors, where the carriers are accreted by a strong electric field, and the process is described as avalanche break down. In graphene photodetectors, the density of photo-excited electron–hole pairs decreases with increasing doping level, which is consistent with electron–electron scattering. Accordingly, photovoltaic current often decreases with distance from the charge neutrality point. It is only pronounced for low-doped samples. Photocurrents arising from a photovoltaic effect are very suitable for high-speed operation due to high carrier mobility.[28,29]

3.2. Photo-thermoelectric effect

In a photo-thermoelectric process, incident light produces a temperature gradient in the device. For a (quasi-)uniformly doped channel, the electrodes serve as a good heat sink, and the temperature gradient is always located at the graphene-metal junction. With this temperature gradient, the thermoelectric photoresponse RTE $\sim \sigma S/\kappa$, where S is the Seebeck coefficient, and σ and κ are the electrical and thermal conductivities, respectively. Due to graphene's large thermal conductivity, the thermoelectric effect is not significant at graphene/metal contacts. Obviously, large thermoelectric photocurrent can be expected in other 2D materials whose high electrical conductivity coincides with low thermal conductivity.

Alternatively, pronounced thermoelectric photocurrent can be generated in graphene by hot carriers.[21,30,31] In this scenario, photo-excited electron–hole pairs lead to ultrafast ($\sim$ 10 fs) heating of carriers in graphene through strong electron–electron interactions. Because the optical phonon energy in graphene is relatively high, the carriers can maintain a temperature much higher than that of the lattice temperature for a few picoseconds before relaxation by lattice phonons starts. Also, because of the slow scattering rate between electron and acoustic phonons, final thermal equilibration of hot carriers in graphene can be prolonged to a timescale up to nanoseconds.[30] Therefore, the temperature differences between carriers is able to produce a significant photo-response by Seebeck effect, instead of that generated by the lattice temperature gradient discussed above. Photo-response resulting from hot carriers rather than the heating of the lattice permits a wide bandwidth. The operating speed is ultrafast, as in the case of photovoltaic photodetectors.

3.3. Bolometric effect

In a bolometric process, heating by incident light results in a differential change in the conductivity of the channel.[32] It is worth mentioning that the bolometric effect is a photoconductive process, i.e., instead of generating photocurrent under zero-bias, it only modifies the conductance of graphene under external bias. Bolometric responsivity is characterized by the bolometric coefficient, which is the sensitivity of electrical conductivity with the temperature, i.e., $\beta = \mathrm{d}\sigma/\mathrm{d}T$. The conductivity change induced by light heating can be divided into two parts: temperature-dependent carrier mobility and change of carrier densities. Bolometric effect supports detecting long wavelength light even up to submillimeter wavelength range.[33]

In contrast to the photovoltaic effect, the thermoelectric effect and bolometric effect produce similar photo-current polarity, which is the opposite of conduction current. Photo-thermoelectric effect is significant only around the graphene (2D material)/metal contact or p–n junction interface, and its photo-response is proportional to the incident light power. The bolometric phenomenon is extremely pronounced in high-bias cases. The largest photo-current is obtained when the incident light is focused at the center of the channel, and the photo-response increases nearly linearly with the source–drain bias.

3.4. Plasma-wave-assisted terahertz detection

Nanoscale FET is able to detect THz radiation through plasma-wave rectification: a d.c. output signal is generated in response to collective carrier density oscillations (plasma waves). This is because of a driving longitudinal electric field along the channel resulting from the coupling of electromagnetic waves between the source and gate (plasma waves launched at the source). This effect was first proposed by Dyakonov and Shur.[34] Owing to its high carrier mobility, graphene is a promising candidate for room-temperature-operated, plasma-wave-assisted THz detectors. A typical THz detector based on a top-gate antenna-coupled configuration was reported in Ref. [35] A maximum responsivity of 1.3 V/W or 1.3 mA/W was demonstrated at 0.3 THz.[35] So far, plasma-assisted graphene detectors have not been successfully integrated with silicon photonics. In the following sections, we will focus our discussion on integrated devices; we refer the reader to another general review for details of plasma-wave-assisted detectors.[16]

3.5. Photogating effect

In addition to the 'intrinsic' photo-response discussed in the previous sections, photo-response can be generated by

charge trapping of trap centers or charge transfer between graphene and other materials. In the photogating effect, one type of photo-generated carrier is captured by the external trap centers (or transferred from external sources).[36–40] This charge transfer process results in a change of carrier density in graphene channels. As a result, incident light modifies the channel conductivity. Photogating is also a photoconductive process, and its photo-current polarity is determined by charge trap types or charge transfer directions. Photo-induced carriers can transport several times through the channel before their recombination, providing a significant optical gain, so the responsivity resulting from the photogating effect can be very large, up to millions of A/W. For comparison, responsivity in the photo-thermoelectric and bolometric regimes is limited to less than a few mA/W. Obviously, longer photo-carrier lifetime means larger photo-gain and higher responsivity, but at the cost of lower operating speed. Photogating effect is generally significant for small incident light power. It always saturates with increasing light power. The saturation threshold power is controlled by the density of trapping centers.

4. State-of-the-art graphene integrated photodetectors

Monolayer graphene absorbs $\sim 2.3\%$ of incident light, which is very small in total absorption, although the light–matter interaction is surprisingly strong within one-atom geometric thickness.[41] As a consequence, the overall responsivity of conventional graphene photodetectors is limited by their low absorption (typically a few mA/W). Practically, enhancing optical absorption and responsivity is highly desired and is one of the key challenges in graphene photodetectors. A plasmonic antenna can be used to increase absorption, but its sharp resonant absorption limits the spectral bandwidth.[42,43] Decorating graphene with light absorbers (such as quantum dots or perovskite) is an alternative way; high photogain can be obtained through a photogating effect, but at the cost of lower operating speed.[36,37]

4.1. Integrated with optical cavity

Light absorption can be significantly promoted by embedding graphene into optical or photonic crystal cavities. An optical cavity always comprises a thin dielectric layer encapsulated by two mirrors (either Bragg or metallic reflectors).[44,45] The thickness is configured as a quarter of the resonant wavelength. As a result, the optical field is trapped inside the cavity, so light passes through the embedded graphene sample several times. In this way, light absorption is significantly increased in a compact device. The quality factor of an optical cavity sets a trade-off between optical bandwidth and absorption enhancement. Furchi *et al.* integrated a metal/graphene/metal (MSM) detector with a Bragg-mirror-based micro cavity (Fig. 2(a)). A 26-fold light absorption enhancement was obtained, resulting in responsivity of 21 mA/W. Because Bragg mirrors provide optical confinement only in the vertical direction, the quality factor is relatively low, resulting in limited absorption enhancement. On the other hand, a photonic crystal cavity permits a very high quality factor, because, by means of in-plane Bragg reflections of periodic micro structures and total internal reflections in the perpendicular directions, light is confined in three dimensions (Fig. 2(b)).[46] An MSM photodetector can be fabricated by transferring graphene followed by strand etching, patterning, and metallization processes.[47] The structure provides giant light–matter interaction and a favorable device footprint, at the expense of reducing operating bandwidth due to the sharp resonant peak of the photonic crystal cavity.

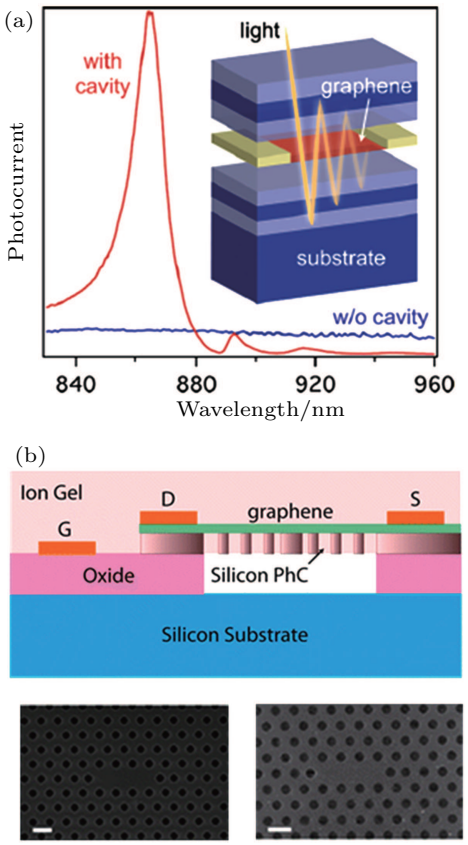


Fig. 2. (color online) Micro-optical-cavity integrated graphene photodetector. (a) Spectral response of a bi-layer graphene device integrated with a silicon optical cavity. Measurements of responsivity with and without the cavity. Without the cavity, the photoresponse is flat in wavelength and more than an order of magnitude lower than that with the cavity. Inset: Schematic of a graphene microcavity photodetector. Distributed Bragg mirrors form a high-fitness optical cavity. Incident light is trapped in the cavity and passes through the graphene repeatedly. The graphene sheet is shown in red, and the metal contacts are in yellow (from Ref. [45]). (b) Top: Schematic of an electrically tunable graphene device integrated with a silicon nanocavity. Bottom: Scanning electron micrographs showing the silicon cavity before (left) and after (right) graphene transfer (from Ref. [46]).

4.2. Integrated with silicon waveguide

Alternatively, light absorption by graphene can be enhanced by integrating graphene photodetectors with low-loss

optical waveguides. In this scenario, the evanescent mode of optical electric field is confined and guided by the waveguides, propagating parallel to graphene channels. Consequently, light interacts with graphene during its travelling in the waveguide, resulting in graphene absorbing light in the entire length in the in-plane direction. This interaction behavior is fundamentally different from the traditional far-field coupling where light interacts with graphene only within one atomic length out-of-plane, maximizing the optical absorption. Li *et al.* measured the light absorption of a graphene-integrated silicon waveguide based on a Mach–Zender interferometer.[48] They revealed that the absorption coefficient is as high as 0.2 dB/μm in this configuration, which means that the light absorption can be enhanced up to 50% (90%) in a 15 μm (50 μm) long graphene sample.

Gan *et al.* demonstrated a graphene MSM photodetector with a pair of asymmetric electrodes fabricated parallel to but at different distances from the waveguide, as shown in Fig. 3(a). The asymmetric electrical potential separates photo-generated electro–hole pairs, resulting in photo-current.[49] A flat responsivity around 0.1 A/W (in 53 μm long waveguide) was obtained with zero bias in the 1450–1590 nm wavelength. At the same time, Pospischil *et al.* fabricated an integrated photodetector by placing one entire electrode on the waveguide, and the other electrode a few micrometers away from the waveguide, as illustrated in Fig. 3(b).[50] They obtained 0.05 A/W responsivity (in a 24 μm long waveguide) in a broad band (covering O- to U- telecommunication band). Graphene photodetectors also permit an ultrahigh operating speed due to exceptionally high carrier mobility. Gan *et al.* examined the high-speed response of their photodetector. Bandwidth over 20 GHz and a clear open eye diagram at 12 Gbit/s were measured.[49] Later, the data rate was further pushed to 50 Gbp/s in similar detectors fabricated by a scalable process.[51] The overall performance can be further improved with high quality graphene samples[52] or sophisticated waveguide structures.[53,54] For example, Shiue *et al.* fabricated a graphene integrated photodetector by using boron-nitride encapsulated graphene structures.[52] Benefitting from improved graphene quality (in terms of carrier transport properties), 0.36 A/W responsivity and 42 GHz bandwidth were achieved.

On the other hand, a graphene integrated photodetector can be enhanced by forming graphene/silicon heterostructures. Wang *et al.* demonstrated a graphene/silicon hetero-photodetector naturally integrated with silicon waveguide on SOI substrate, which is schematically shown in Fig. 4(a).[55] The authors obtained 0.13 A/W responsivity at mid-IR range (2.75 μm wavelength). In addition, the Schottky barrier between graphene and silicon effectively suppresses dark current and noise at room temperature. In this scenario, the fabricated photodetector does not require cryocooling during operation, which is practically desirable but has not been achieved in traditional narrow bandgap compound semiconductors. The extension of spectral range and the capability of working at room temperature render the detector very suitable for important mid-IR applications such as chemical sensing, infrared imaging, and on-chip spectroscopy. Moreover, avalanche breakdown in silicon may further increase photo responsivity. Goykhman *et al.* reported an integrated graphene–silicon Schottky photodetector. The device achieved responsivity up to 0.37 A/W for 1.5 μm incident light at high reverse biases due to avalanche multiplication (Figs. 4(b) and 4(c)).[56]

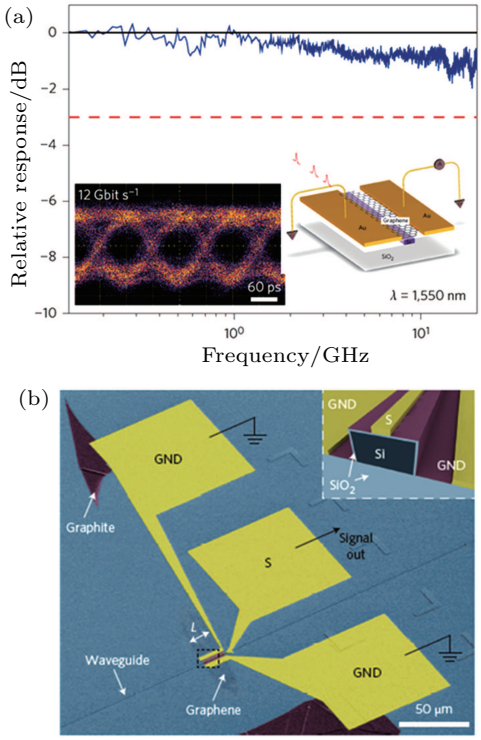


Fig. 3. (color online) Silicon waveguide-integrated graphene photodetectors. (a) The relative a.c. photoresponse as a function of light intensity modulation frequency shows 1 dB degradation of the signal at frequency 20 GHz. Inset (left) 12 Gbit/s optical data link test of the device, showing a clear eye opening, (right) schematic of the device. The silicon bus waveguide fabricated on an SOI wafer is planarized using SiO_2. A graphene layer is transferred onto the planarized waveguide with a spacing layer of $\sim$ 10 nm SiO_2. Two metal electrodes contact the graphene and conduct the generated photocurrent. One of the electrodes is closer to the waveguide to create a potential difference in the graphene to couple with the evanescent optical field of the waveguide (from Ref. [49]). (b) Colored scanning electron micrograph of a waveguide-integrated graphene photodetector. The "active region" of the graphene sheet is shown in violet. Inset shows a cross-section of the device. The graphene sheet coats both the top surface and sidewalls of the waveguide. A thin SiO_2 layer prevents electrical contact between the graphene and the silicon waveguide (from Ref. [50]).

In the waveguide configurations, optimization of a practical device involves performance trade-offs. A relatively long sample length was used, which increases the device footprint and fabrication cost. In addition, larger sample size simply means higher parasitic capacitors, which decrease the operating speed.

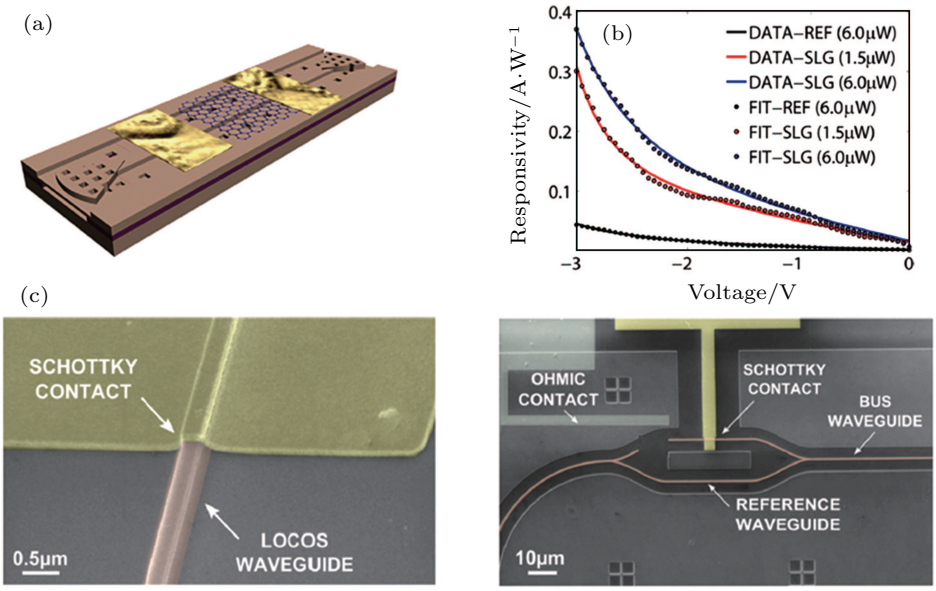


Fig. 4. (color online) Integrated graphene/silicon heterostructure photodetector. (a) Schematic of graphene/silicon heterostructure waveguide photodetector. The photodetector is formed by a graphene/silicon heterojunction on an SOI waveguide. Electrodes and focusing sub-wavelength grating are also demonstrated (from Ref. [55]). (b) Responsivity of graphene silicon and reference metal silicon Schottky photodetector, showing the photogain under negative bias conditions. Colored solid lines show a fit of the bias-dependent responsivity based on combined thermionic-field emission and avalanche multiplication process. (c) SEM micrograph of graphene silicon Schottky photo-detector. (Left) Graphene is coupled to a waveguide. (Right) Layout of the complete device (from Ref. [56]).

5. Toward full suite of 2D integrated photonics

An optical interconnect involves several active devices – at least modulators, lasers, and photodetectors. Advanced SOI interconnection requires improving all constituent components of a photonic data transmission system on the SOI platform. It is worth mentioning that the unique optical properties of graphene and other 2D materials enable many important integrated optoelectric devices, not only graphene photodetectors.[57–59]

Actually, the idea of integrating graphene with silicon photonics was first proposed and implemented in optical modulators. Liu integrated large-scale, monolayer graphene with a silicon waveguide. By adjusting the doping level of graphene, its optical absorption was electrically modulated (by either metal or graphene top gate), forming a broadband optical modulator covering the telecommunication range of 1.3–1.6 μm (Figs. 5(a) and 5(b)).[60,61] Youngblood fabricated a multifunctional photodetector by integrating a graphene field-effect transistor on top of a silicon waveguide.[62] A graphene top gate was used to modulate the light absorption of another graphene channel at the bottom. At the same time, the photoresponse of the bottom graphene channel was used as a photodetector. In addition to electrical modulation, photoabsorption of graphene can be adjusted by another light through optically induced transparency. Yu *et al.* demonstrated light controlled transmission in a graphene integrated silicon waveguide device, mimicking a full optical modulator.[63] Sophisticated modulators can also be obtained by combining a silicon waveguide with other complex structures, to shrink device sizes and increase operating speed. Two groups demonstrated enhanced modulation depth by employing micro-ring resonators in the silicon waveguide chips. The devices exhibited more efficient amplitude modulation.[64,65] Alternatively, Gao *et al.* reported an electro-optic modulator by integrating graphene/hBN stacking with a photonic crystal nanocavity.[66]

Moreover, graphene is a gapless material. Its semimetallic nature impedes the realization of other necessary optical components for interconnection or telecommunication, such as on-chip light sources. Fortunately, the family of 2D materials has rich physical properties. Using other 2D materials may fill the application gaps. For example, monolayer TMDCs are direct bandgap materials and present exceptional excitonic and quantum emission properties.[67] An important merit of TMDC monolayers is their large exciton binding energy resulting from substantially reduced screening.[68] This leads to excitons with a long lifetime that are very suitable for light emission applications. Recently, a few groups independently explored the possibility of fabricating laser diodes by TMDCs, as demonstrated in Figs. 5(c) and 5(d). By integrating TMDCs with micro-disk resonators or photonic crystal cavities, they successfully demonstrated amplified spontaneous emission,[69] and eventually approached coherent light sources.[70–72] Black phosphorus is another instance. It is a direct bandgap material regardless of the number of its layers. It possesses a wide-range tunable bandgap (0.3 eV in bulk form to 2 eV in monolayer), offering potentially high light–matter interaction in mid-IR range. Recently, black phosphorus was proposed to implement a high-performance integrated modulator.[73]

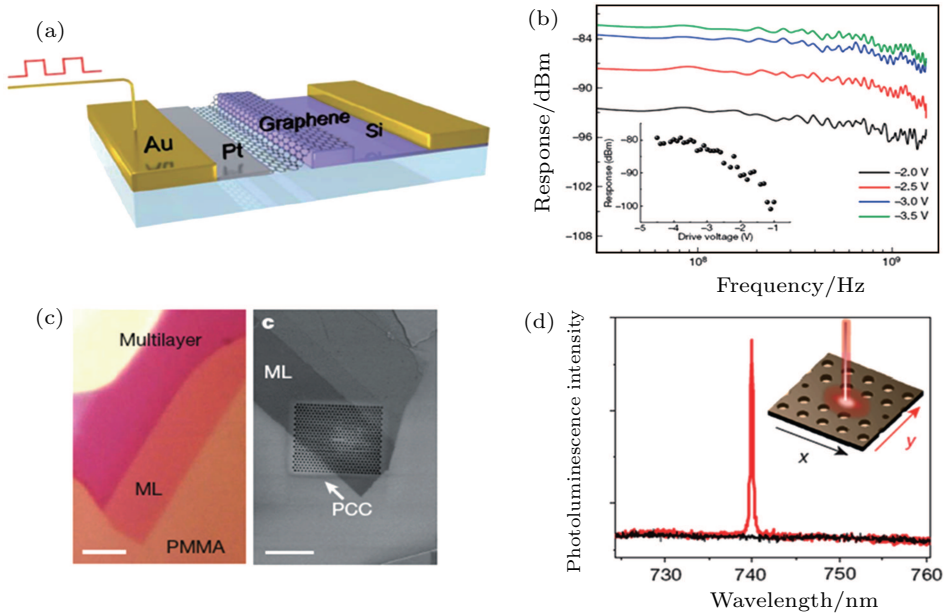


Fig. 5. (color online) Integrated 2D materials/silicon modulator and light source. (a) Three-dimensional schematic illustration of the graphene-based, waveguide-integrated, optical modulator. A monolayer graphene sheet is on top of a silicon bus waveguide, separated from it by a 7-nm AlO_x layer. The silicon waveguide is connected to the electrode through a thin layer of silicon defined by selective etching. (b) Dynamic electro-optical response of the graphene waveguide modulator. The main panel shows the response of the device as a function of frequency at different drive voltages. The measured 3-dB bandwidths of the device are between 0.8 GHz and 1.2 GHz. Inset: Low-frequency device response with different drive voltages, indicating that the device has best performance at a drive voltage of −4 V (from Ref. [60]). (c) (Left) Optical image of monolayer WSe_2 on PMMA before transfer to photonic crystal cavity. (Right) Scanning electron micrograph of the hybrid monolayer WSe_2-photonic crystal cavity nanolaser. (d) Polarization-resolved photoluminescence spectrum of the hybrid laser taken at 80 K, showing a completely polarized narrow emission at ∼ 740 nm. Black (red) line corresponds to detected linear polarization in the x (y) direction (from Ref. [69]).

6. Conclusion and prospects

Technically, passive and active silicon integrated with graphene and other 2D semiconductors have emerged as promising candidates for a wide range of applications. Their remarkable performance has breathed new life into the rapid development of silicon-integrated photonics. Based on graphene integrated silicon photonic structures, photodetectors have outstanding merits including high responsivity covering a broad spectral range, and fast operation, which give silicon optical chips great potential and new opportunities in a variety of applications. Despite the rapid progress in this area, further work is needed both in fundamental and technological sides from a practical viewpoint.

First, an important question is whether the hybrid silicon/2D platform will be a fully functional platform. In addition to already-demonstrated photodetectors, this would require further optimizing the photodetectors as well as developing other integrated photonic devices, including modulators and on-chip light sources. The development of silicon/2D integrated photonic devices is still in its infancy; improved performance can be expected from introducing other sophisticated nano-photonic techniques into the devices. For instance, the plasmon is a powerful tool to facilitate light in nano-scale. Using excitation of surface plasmons (localized plasmon or surface plasmon–polariton), the electric field can be further concentrated around 2D materials, increasing photoresponse. Alternatively, taking advantage of the rich optical properties of plasmon, performance of modulators and emitters can be boosted. Second, as already mentioned, the large family of 2D materials provides a wide range of material properties, offering flexibility in designing devices to fit diverse application requirements. The variety of available 2D materials with vdW heterostructures may enable great future research on integrated photonics.

References

[1] Hochberg M and Baehr J T 2010 *Nat. Photon.* **4** 492
[2] Soref R 2006 *IEEE J. Sel. Topics in Quantum Electron.* **12** 1678
[3] Izhaky N, Morse M, Koehl S, Cohen O, Rubin D, Barkai A, Sarid G, Cohen R and Paniccia M 2006 *IEEE J. Sel. Topics in Quantum Electron.* **12** 1688
[4] Jalali B and Fathpour S 2006 *IEEE J. Lightwave Technol.* **24** 4600
[5] Jokerst N M, Brooke M A, Cho S Y, Thomas M, Lillie J, Kim D, Ralph S, Dennis K, Comeau B and Henderson C 2005 *Proc. SPIE* **5730** 226
[6] Hu J, Sun X, Agarwal A and Kimerling L C 2009 *J. Opt. Soc. Am. B* **26** 1032
[7] Roelkens G, Liu L, Liang D, Jones R, Fang A, Koch B and Bowers J 2010 *Laser Photon. Rev.* **4** 751
[8] Heck M, Chen H W, Wang A, Koch B, Liang D, Park H, Sysak M and Bowers J 2011 *IEEE J. Sel. Topics in Quantum Electron.* **17** 333
[9] Soref R 2010 *Nat. Photon.* **4** 495
[10] Xia F, Wang H, Xiao D, Dubey M and Ramasubramaniam A 2014 *Nat. Photon.* **8** 899
[11] Mak K F, Ju L, Wang F and Heinz T F 2012 *Solid State Commun.* **152** 1341
[12] Xia F, Yan H and Avouris P 2013 *Proceedings of the IEEE* **101** 1717
[13] Geim A K and Novoselov K S 2007 *Nat. Mater.* **6** 183
[14] Geim A K 2009 *Science* **324** 1530
[15] Freitag M, Low T, Xia F and Avouris P 2013 *Nat. Photon.* **7** 53
[16] Koppens F H L, Mueller T, Avouris P, Ferrari A C, Vitiello M S and Polini M 2014 *Nat. Nano* **9** 780
[17] Li J, Niu L, Zheng Z and Yan F 2014 *Adv. Mater.* **26** 5239

[18] Lee E J H, Balasubramanian K, Weitz R T, Burghard M and Kern K 2008 *Nat. Nano* **3** 486
[19] Park J, Ahn Y H and Ruiz V C 2009 *Nano Lett.* **9** 1742
[20] Liu N, Tian H, Schwartz G, Tok J B H, Ren T L and Bao Z 2014 *Nano Lett.* **14** 3702
[21] Gabor N M, Song J C W, Ma Q, Nair N L, Taychatanapat T, Watanabe K, Taniguchi T, Levitov L S and Jarillo H P 2011 *Science* **334** 648
[22] Wang X, Xie W, Chen J and Xu J B 2014 *ACS Appl. Mat. Interfaces* **6** 3
[23] George P A, Strait J, Dawlaty J, Shivaraman S, Chandrashekhar M, Rana F and Spencer M G 2008 *Nano Lett.* **8** 4248
[24] Sun D, Wu Z K, Divin C, Li X, Berger C, de Heer W A, First P N and Norris T B 2008 *Phys. Rev. Lett.* **101** 157402
[25] Kim R, Perebeinos V and Avouris P 2011 *Phys. Rev. B* **84** 075449
[26] Winzer T, Knorr A and Malic E 2010 *Nano Lett.* **10** 4839
[27] Tielrooij K J, Song J C W, Jensen S A, Centeno A, Pesquera A, Zurutuza Elorza A, Bonn M, Levitov L S and Koppens F H L 2013 *Nat. Phys.* **9** 248
[28] Xia F, Mueller T, Lin Y m, Valdes G A and Avouris P 2009 *Nat. Nanotechnol.* **4** 839
[29] Mueller T, Xia F and Avouris P 2010 *Nat. Photon.* **4** 297
[30] Bistritzer R and MacDonald A H 2009 *Phys. Rev. Lett.* **102** 206410
[31] Song J C W, Rudner M S, Marcus C M and Levitov L S 2011 *Nano Lett.* **11** 4688
[32] Yan J, Kim M H, Elle J A, Sushkov A B, Jenkins G S, Milchberg H M, Fuhrer M S and Drew H D 2012 *Nat. Nano* **7** 472
[33] Cai X, Sushkov A B, Suess R J, Jadidi M M, Jenkins G S, Nyakiti L O, Myers W R L, Li S, Yan J, Gaskill D K, Murphy T E, Drew H D and Fuhrer M S 2014 *Nat. Nano* **9** 814
[34] Dyakonov M and Shur M 1996 *IEEE Transactions on Electron Devices* **43** 380
[35] Vicarelli L, Vitiello M S, Coquillat D, Lombardo A, Ferrari A C, Knap W, Polini M, Pellegrini V and Tredicucci A 2012 *Nat. Mater.* **11** 865
[36] Konstantatos G, Badioli M, Gaudreau L, Osmond J, Bernechea M, de Arquer F P G, Gatti F and Koppens F H L 2012 *Nat. Nano* **7** 363
[37] Lee Y, Kwon J, Hwang E, Ra C H, Yoo W J, Ahn J H, Park J H and Cho J H 2015 *Adv. Mat.* **27** 41
[38] Liu Y 2015 *Nat. Commun.* **6** 8589
[39] Zhang D, Gan L, Cao Y, Wang Q, Qi L and Guo X 2012 *Adv. Mat.* **24** 2715
[40] Sun Z, Liu Z, Li J, Tai G A, Lau S P and Yan F 2012 *Adv. Mat.* **24** 5878
[41] Nair R R, Blake P, Grigorenko A N, Novoselov K S, Booth T J, Stauber T, Peres N M R and Geim A K 2008 *Science* **320** 1308
[42] Echtermeyer T J, Britnell L, Jasnos P K, Lombardo A, Gorbachev R V, Grigorenko A N, Geim A K, Ferrari A C and Novoselov K S 2011 *Nat. Commun.* **2** 458
[43] Liu Y, Cheng R, Liao L, Zhou H, Bai J, Liu G, Liu L, Huang Y and Duan X 2011 *Nat. Commun.* **2** 579
[44] Engel M, Steiner M, Lombardo A, Ferrari A C, Löhneysen H V, Avouris P and Krupke R 2012 *Nat. Commun.* **3** 906
[45] Furchi M, Urich A, Pospischil A, Lilley G, Unterrainer K, Detz H, Klang P, Andrews A M, Schrenk W, Strasser G and Mueller T 2012 *Nano Lett.* **12** 2773
[46] Majumdar A, Kim J, Vuckovic J and Wang F 2013 *Nano Lett.* **13** 515
[47] Shiue R J, Gan X, Gao Y, Li L, Yao X, Szep A, Walker D, Hone J and Englund D 2013 *Appl. Phys. Lett.* **103** 241109
[48] Li H, Anugrah Y, Koester S J and Li M 2012 *Appl. Phys. Lett.* **101** 111110
[49] Gan X, Shiue R J, Gao Y, Meric I, Heinz T F, Shepard K, Hone J, Assefa S and Englund D 2013 *Nat. Photon.* **7** 883
[50] Pospischil A, Humer M, Furchi M M, Bachmann D, Guider R, Fromherz T and Mueller T 2013 *Nat. Photon.* **7** 892
[51] Schall D, Neumaier D, Mohsin M, Chmielak B, Bolten J, Porschatis C, Prinzen A, Matheisen C, Kuebart W, Junginger B, Templ W, Giesecke A L and Kurz H 2014 *ACS Photon.* **1** 781
[52] Shiue R J, Gao Y, Wang Y, Peng C, Robertson A D, Efetov D K, Assefa S, Koppens F H L, Hone J and Englund D 2015 *Nano Lett.* **15** 7288
[53] Wang J, Cheng Z, Chen Z, Wan X, Zhu B, Tsang H K, Shu C and Xu J 2016 *Nanoscale* **8** 13206
[54] Zhou H, Gu T, McMillan J F, Yu M, Lo G, Kwong D L, Feng G, Zhou S and Wong C W 2016 *Appl. Phys. Lett.* **108** 111106
[55] Wang X, Cheng Z, Xu K, Tsang H K and Xu J B 2013 *Nat. Photon.* **7** 888
[56] Goykhman I, Sassi U, Desiatov B, Mazurski N, Milana S, de Fazio D, Eiden A, Khurgin J, Shappir J, Levy U and Ferrari A C 2016 *Nano Lett.* **16** 3005
[57] Kim K, Choi J Y, Kim T, Cho S H and Chung H J 2011 *Nature* **479** 338
[58] Sun Z, Martinez A and Wang F 2016 *Nat. Photon.* **10** 227
[59] Mak K F and Shan J 2016 *Nat. Photon.* **10** 216
[60] Liu M, Yin X, Ulin A E, Geng B, Zentgraf T, Ju L, Wang F and Zhang X 2011 *Nature* **474** 64
[61] Liu M, Yin X and Zhang X 2012 *Nano Lett.* **12** 1482
[62] Youngblood N, Anugrah Y, Ma R, Koester S J and Li M 2014 *Nano Lett.* **14** 2741
[63] Yu L, Zheng J, Xu Y, Dai D and He S 2014 *ACS Nano* **8** 11386
[64] Qiu C, Gao W, Vajtai R, Ajayan P M, Kono J and Xu Q 2014 *Nano Lett.* **14** 6811
[65] Ding Y, Zhu X, Xiao S, Hu H, Frandsen L H, Mortensen N A and Yvind K 2015 *Nano Lett.* **15** 4393
[66] Gao Y, Shiue R J, Gan X, Li L, Peng C, Meric I, Wang L, Szep A, WalkerJr D, Hone J and Englund D 2015 *Nano Lett.* **15** 2001
[67] Wang Q H, Kalantar Z K, Kis A, Coleman J N and Strano M S 2012 *Nat. Nano* **7** 699
[68] Xu X, Yao W, Xiao D and Heinz T F 2014 *Nat. Phys.* **10** 343
[69] Reed J C, Zhu A Y, Zhu H, Yi F and Cubukcu E 2015 *Nano Lett.* **15** 1967
[70] Wu S, Buckley S, Schaibley J R, Feng L, Yan J, Mandrus D G, Hatami F, Yao W, Vuckovic J, Majumdar A and Xu X 2015 *Nature* **520** 69
[71] Ye Y, Wong Z J, Lu X, Ni X, Zhu H, Chen X, Wang Y and Zhang X 2015 *Nat. Photon.* **9** 733
[72] Salehzadeh O, Djavid M, Tran N H, Shih I and Mi Z 2015 *Nano Lett.* **15** 5302.
[73] Lin C, Grassi R, Low T and Helmy A S 2016 *Nano Lett.* **16** 1683